Pergamon

Int. J. Radiation Oncology Biol. Phys., Vol. 33, No. 5, pp. 1127–1138, 1995

0360-3016/95 $9.50 + .00

0360-3016(95)00257-X

● *Treatment Planning and Plan Evaluation*

COMPUTER-AIDED DESIGN AND FABRICATION OF AN ELECTRON BOLUS FOR TREATMENT OF THE PARASPINAL MUSCLES

DANIEL A. LOW, PH.D.,*,‡ GEORGE STARKSCHALL, PH.D.,* NEIL E. SHERMAN, M.D.,†,§ STANLEY W. BUJNOWSKI, M.S.,* JAMES R. EWTON, B.S.* AND KENNETH R. HOGSTROM, PH.D.*

Departments of *Radiation Physics and †Radiotherapy, The University of Texas M.D. Anderson Cancer Center, Houston TX 77030

Purpose: demonstrate the technology for the design, fabrication, and verification of an electron bolus used in the preoperative irradiation of a mesenchymal chondrosarcoma in the paraspinal muscle region (T8–T12), in which the target volume overlay a portion of the spinal cord, both lungs, and the right kidney.
Methods and Materials: An electron-bolus design algorithm implemented on a three dimensional (3D) radiotherapy treatment planning system designed the bolus to yield a dose distribution that met physician-specified clinical criteria. Electron doses were calculated using a 3D electron pencil-beam dose algorithm. A computer-driven milling machine fabricated the bolus from modeling wax, machining both the patient surface and the beam surface of the bolus. Verification of the bolus fabrication was achieved by repeating the patient's computed tomography (CT) scan with the fabricated bolus in place (directly on the posterior surface of the prone patient) and then recalculating the patient's dose distribution using the 3D radiotherapy treatment planning system.
Results: A treatment plan using a 17-MeV posterior electron field with a bolus delivered a superior dose distribution to the patient than did the same plan without a bolus. The bolus plan delivered a slightly increased dose to the target volume as a result of a slightly broader range of doses. There were significant reductions in dose to critical structures (cord, lungs, and kidney) in the bolus plan, as evidenced by dose–volume histograms (DVHs). The patient dose distribution, calculated using CT scan data with the fabricated bolus, showed no significant differences from the planned dose distribution.
Conclusions: A bolus can provide considerable sparing of normal tissues when using a posterior electron beam to irradiate the paraspinal muscles. Bolus design and fabrication using the tools described in this paper are adequate for patient treatment. CT imaging of the patient with the bolus in place followed by calculation of the patient's dose distribution demonstrated a useful method for verification of the bolus design and fabrication process.

Electron conformal radiotherapy, Electron bolus, Three dimensional treatment planning, Sarcoma of paraspinal muscles.

INTRODUCTION

Irradiation using electron beams has been advocated for treatment of sarcomas of the paraspinal muscles to deliver a desired dose to the superficial target volume, while sparing uninvolved structures such as lung and spinal cord (5). Because the depth of the distal surface of the target volume varies across the treatment field, the requirement that the target volume be irradiated to the therapeutic dose can result in the undesired overirradiation of distal critical structures. The use of a beam with spatially varying incident mean energy and corresponding therapeutic range can achieve this goal. This spatial energy modulation can be effected for electron or other charged-particle beams by the use of bolus material of an appropriately varying thickness placed on the patient's body.

Techniques to automate the design and fabrication of boluses have been used for many years in heavy-particle radiotherapy (7, 17). The use of a bolus for these modalities has allowed a significant flexibility and precision in the positioning of the dose distribution relative to the target volume and nearby critical structures. Low *et al.*

Reprint requests to: Daniel A. Low, Ph.D., Division of Radiation Oncology, Mallinckrodt Institute of Radiology, 510 South Kingshighway, St. Louis, MO 63110. E-mail: low@castor.wustl.edu.
Acknowledgements— This work was supported in part by NCI Grant CA-06294.

‡ Present address: Division of Radiation Oncology, Mallinckrodt Institute of Radiology, 510 South Kingshighway, St. Louis, MO 63110.
§ Present address: Department of Radiation Therapy, Memorial City Medical Center, 920 Frostwood, Houston, TX 77024.
Accepted for publication 26 May 1995.

(10) have developed a methodology for computer-aided electron-bolus design that differs from that used for heavy particles in that it accounts for multiple Coulomb scattering. This methodology has been implemented into a three dimensional (3D) radiotherapy treatment planning system (RTP) that uses a 3D electron pencil-beam dose model (6, 15). The 3D-RTP system was networked with a computer-driven milling machine (9) system that mills boluses from resin-impregnated wax (8).

The purpose of this paper is to report on the first clinical use of this bolus design and fabrication system, and to thus demonstrate the usefulness of an electron bolus in reducing the dose to uninvolved critical structures in treatment of the paraspinal muscles. Also, a method for verification of the resulting patient dose distribution, by recalculating the dose using computed tomography (CT) scan data of the patient with the bolus in place, is demonstrated.

METHODS AND MATERIALS

Treatment aim

A 17-year-old woman was diagnosed to have mesenchymal chondrosarcoma of the right posterior paraspinal muscle at the level from T8 to T12, with possible microscopic extension to the contralateral side, but no metastatic disease. She received three cycles of CyADIC chemotherapy with a partial response. The patient was to undergo external-beam radiotherapy prior to surgical excision of the tumor. The tumor was 11×9.5 cm^2 in dimension perpendicular to the beam and was treated by an approximately 23×14 cm^2 field with corner blocks. The target volume overlay parts of both lungs, the right kidney, and the spinal cord. Because of the patient's young age and favorable prognosis, care was taken to spare as much of the lungs and spinal cord as possible.

A dose to the target volume of 50 Gy in 25 fractions was prescribed. The original prescription specified a given dose of 44.4 Gy using 15-MeV electrons, subsequently modified to 17-MeV electrons (40 Gy to the 90% isodose surface) combined with a given dose of 11.1 Gy using 6 MV x-rays (10 Gy at 4.5 cm). (The term *given dose* is defined here as the dose delivered to a miniphantom of muscle in a water phantom, located at the depth of maximum dose on the central axis of a rectangular field that just encompasses the blocked field; the water phantom has the same source-to-surface distance as prescribed for the patient.) The purpose of the x-ray treatment was to limit the amount of dose to the skin. The electron dose was to be delivered 4 days of each week, and the x-ray dose was to be delivered on 1 day; both delivered at 2.22 Gy per fraction. Both fields were oriented posteriorly, with the patient in the prone position. The maximum dose in the target volume was to be limited to 61 Gy, 110% of the given dose. The dose to the spinal cord, kidney, and lungs was to be limited to 45 Gy, 25 Gy, and 20 Gy, respectively.

Due to practical clinical issues, the actual treatment deviated from the dose plan presented here, and for which the bolus was designed. For illustrative purposes we present only the bolus planned dose distributions. The patient's electron:photon fractions were 18:7 as opposed to 20:5 originally prescribed and presented in the plan. For the 18 electron fractions, the patient received 2 at 15 MeV with no bolus (treatment scheduled prior to bolus fabrication), 4 at 16 MeV, 3 at 17 MeV, and 9 at 20 MeV.

Treatment planning

The patient was first placed in the prone position and a nominal treatment field was temporarily marked on her body's surface. Treatment-planning CT scans were then obtained with a 1-cm slice thickness and a 1-cm spacing encompassing a volume from 5 cm superior to 5 cm inferior to the nominal treatment field. Computed tomography slices at least 3 cm outside the intended field of treatment are necessary for the determination of the patient's body surface beneath the portions of bolus that extend outside the treatment field and for the definition of the patient's anatomy necessary for the calculation of the dose. Contrast-filled catheters were placed on the surface of the patient's body to delineate the nominal treatment field on the CT scans. Subsequently, the physician outlined a target volume on the CT images based on visualization of the tumor and the boundaries of the nominal treatment field. Using the 3D-RTP system, a new treatment field was designed to be 14 cm wide by 23 cm long. The bolus was designed to limit the dose to critical structures that lay distal to the target volume but within the treatment field, while maintaining an acceptably uniform and adequate dose to the target volume. The treatment planning system provided the treatment planner with options to select several bolus-design operators that either generated or altered the bolus shape to achieve the clinical goal (10). The bolus surfaces were described by distances from the virtual source to both the proximal and distal bolus surfaces for each of a set of fanlines. The bolus was designed by the following sequence of operators: the first bolus operator, **P**(0.5, 5.4), designed the bolus so that the physical depth from the proximal bolus surface to the distal surface of the target volume along all fanlines was set to 5.4 cm, which corresponded with the maximum physical depth of the target volume. This operator attempted to enclose the entire target volume within the 90% isodose for a 17-MeV electron beam, which has an R_{90} of 5.5 cm. To ensure that steep spatial gradients of the distal target-volume surface near the perimeter of the projected target volume would not generate a steeply sloped bolus, the initial bolus shape was designed so that the boundary lay 0.5 cm inside the perimeter of the target volume. The first operator created a bowl-shaped bolus surface; the bowl shape was then widened by applying the maximum coverage operator **T**(0.6). This improved lateral coverage of the target volume. Next, the proximal surface of the bolus was extended from the initially designed region to 1 cm outside the treatment field in a

direction perpendicular to the beam's central axis using the bolus extension operator $\mathbf{H}_t$. Finally, small-scale surface features, arising from uneven target-volume definitions, that might contribute to dose inhomogeneities, were removed by applying the Gaussian smoothing operator $\mathbf{S}_t(100, 0.8)$. Using the notation of Low *et al.* (10), the operators used in the bolus design were depicted by the following sequence: $\mathbf{S}_t(100, 0.8)$ $\mathbf{H}_t$ $\mathbf{T}(0.6)$ $\mathbf{P}(0.5, 5.4)$.

Dose calculation

Doses were calculated using The University of Texas M. D. Anderson Cancer Center 3D-RTP System (16). The electron-beam dose distribution was calculated using 3D implementation of the pencil-beam algorithm (15) with a 3D heterogeneity correction on a divergent fanline grid with 0.35-cm spacing at the source to isocenter distance of 100 cm. The photon-beam dose distribution was calculated using the fast Fourier transformation (FFT)-convolution algorithm (18) on a divergent fanline grid with 0.5-cm spacing at the source to isocenter distance. Heterogeneity corrections are implicit in the FFT-convolution algorithm. Dose distributions for each beam are transformed from the beam grid onto a dose grid with 0.35 cm spacing in the patient-centered coordinate system. The dose distributions of each beam were appropriately weighted and combined, producing a displayed isodose.

Dose–volume histograms (DVHs) were calculated for the planning target volume and critical structures were selected by spanning the structures with a specified number of randomly spaced points (11) and calculating the doses to these points by interpolating from the dose grid. Cumulative DVHs were plotted with the dose on the horizontal axis vs. the percentage of the delineated structure's volume irradiated on the vertical axis. The volume of the structure, calculated using Monte Carlo integration coincident with the random selection of points, is displayed along with the DVH.

Bolus fabrication

The bolus was fabricated from a resin-impregnated wax with a physical density of 0.920 ± 0.001 g cm^{-3}, a relative linear collision stopping power of 0.931 ± 0.008, and a relative linear scattering power of 0.731 ± 0.004 (8). The bolus was fabricated using a computer-driven milling machine[1] operated by driving software.[2] The fabrication system, reported by Low *et al.* (9), is similar to those reported by Antolak *et al.* (1) and by Smith *et al.* (14). The mill was limited to a lateral travel of 18 cm by 15 cm, smaller in one direction than the dimension required by the bolus. Therefore, the bolus was milled in two abutting passes, each pass requiring an independent description and tool path. The tool path spacing was nominally 2 mm, using a 4 mm-diameter ball-end mill bit. The proximal bolus surface was machined first, with the unmachined border providing a flat surface on which to lay the bolus when the distal surface was milled. The complete distal surface was machined to match the patient's skin surface. Two-centimeter–thick slabs of wax were attached to the lateral sides of the bolus to increase its structural strength.

Bolus-patient-beam alignment

Accurate and reproducible positioning of the bolus with respect to the beam and to the patient was critical to its use. Scribe lines were placed at the centers of the side faces of the bolus to be matched with the patient-positioning lasers. The patient was placed on the table in the treatment position, using the laser marks to align the patient along the longitudinal and right-left axes. The treatment table was then raised to place the beam's central axis (marked on the patient) at a source-to-surface distance (SSD) of 100 cm. The bolus was placed on the patient, aligning the scribe lines with the positioning lasers. Figure 1 shows a photograph of the bolus on the patient prior to treatment. The scribe lines are visible, as are the patient-positioning laser lines. Because the bolus thickness was 0 cm at the central axis, the skin marks are partially visible.

Comparison of bolus and no bolus treatment plans

The clinical usefulness of the bolus was assessed by comparing dose distributions and DVHs for treatment plans with and without bolus. The comparison is made in view of the treatment aim.

Bolus verification

The bolus design and fabrication process was verified prior to patient treatment. This was accomplished by comparing the dose predicted by the original bolus-design calculations with the dose calculated from a second set of CT images of the patient obtained while the fabricated bolus was in place. This allowed the dose to be calculated without involving the bolus-design algorithms, as the bolus was explicitly included in the CT images. This verifies both proper fabrication and bolus-patient alignment.

The success of the bolus fabrication was evaluated by visually comparing the fabricated bolus shape and resulting distributions with the designed bolus shape and dose distributions. This comparison was performed on all transverse CT images. Three are shown here, one containing the beam's central axis, one 7 cm superior to the central axis, and one 7 cm inferior to the central axis.

RESULTS AND DISCUSSION

Clinical evaluation of treatment plan

The usefulness of the bolus is demonstrated by its ability to provide a dose distribution that better satisfies treat-

[1] CAMM—3 Computer-Aided Modeling Machine, Model PNC-3000, Roland DG Corporation.

[2] SmartCAM Advanced 3-D Modeling, Point Control CO., Eugene, OR.

Fig. 1. A photograph of the patient in the treatment position with the bolus in place. Some of the laser alignment scribe lines are visible, as is the central axis marked on the patient's back at the center of the bolus.

ment aims than does a treatment with no bolus. In all evaluations, the comparisons were between dose distributions and DVHs computed in the absence and presence of a bolus for the electron- and photon-beam irradiation. In both cases, a given dose of 44.4 Gy was delivered via 17 MeV electrons combined with a given dose of 11.1 Gy delivered via 6 MV photons. Isodose lines shown in figures presented in this section indicate the dose delivered in Gy.

Figures 2a and 2b compare dose distributions without and with a bolus, respectively, in the central-axis slice, which contains the region where the distal surface of the target volume was at its deepest. The target-volume coverage on the central-axis slice for the no-bolus treatment plan was similar in many respects to that of the bolus treatment plan. In both cases, coverage of the target volume by the 50 Gy isodose line was inadequate near the spinal cord. This was primarily due to the presence of tumor calcification and the spinous process. However, the sloping walls of the bolus focused scattered electrons in this location for the bolus field, resulting in the 50 Gy isodose more closely conforming to the distal surface of the target volume. The bolus' sloping surface also resulted in increasing the maximum dose to the target volume from 56.6 Gy for the no-bolus plan to 59.2 Gy for the bolus plan; however, this dose remained within acceptable dose bounds. For both the bolus and the no-bolus plans, a small portion of the spinal cord in this transverse plane received a dose in excess of 45 Gy. The bolus resulted in a significant reduction in the dose to the lung, particularly to the left lung. The amount of lung in this transverse plane is small, and a significant amount of lung in this plane received a dose in excess of 40 Gy in the no-bolus plan, whereas the 40 Gy isodose line missed the lung in the bolus plan.

The depth of the target volume was less in the off-axis slices than that in the central-axis slice. The bolus was therefore thicker here than it was near the central axis, and the significance of its use was more pronounced. Figures 3a and 3b show dose distributions without and with a bolus, respectively, in a transverse plane 7 cm superior to the central axis. The target volume was well covered in both cases, with only a small portion of the target volume receiving less than 50 Gy. The sloping walls of the bolus contributed slightly to dose heterogeneity in the target volume, increasing the maximum dose from 55.8 to 60.8 Gy. In the no-bolus plan, the spinal cord was completely enclosed by the 50 Gy isodose, a clinically unacceptable situation, whereas in the bolus plan the 50 Gy line just abutted the posterior border of the cord. The dose to both lungs was significantly decreased with the use of the bolus. The 50 Gy isodose line penetrated 4 cm into the right lung when no bolus was used but penetrated less than 1 cm with the bolus. The 25 Gy isodose showed significant reduction in amount of irradiated lung in the bolus plan. This is better appreciated later in the DVHs.

Figures 4a and 4b show dose distributions without and

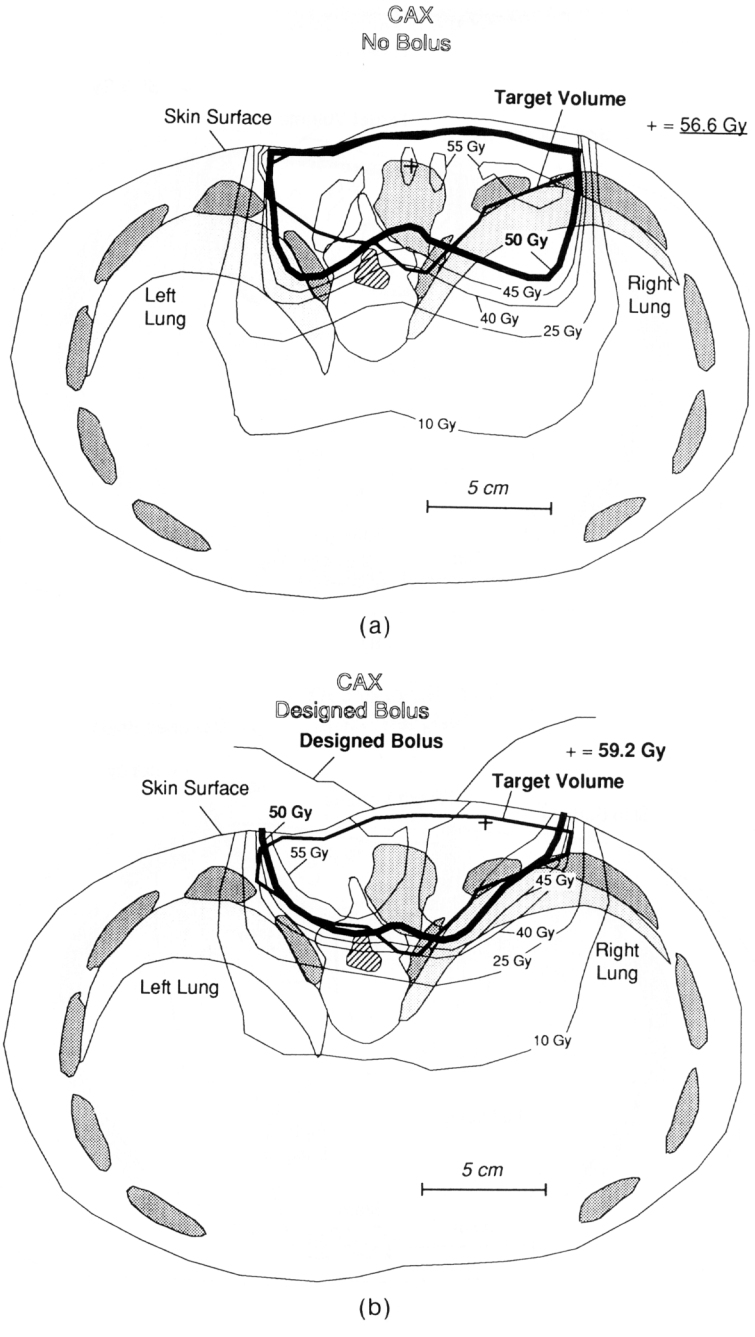

Fig. 2. Comparison of the dose distributions in the transverse plane containing the central axis of the beam. The position of the point of highest dose is identified with a +, and the dose at this point is indicated. (a) The dose distribution was calculated without a bolus. (b) The dose distribution was calculated with the designed bolus.

with a bolus, respectively, in a transverse plane 7 cm inferior to the central axis of the beam. Here the lungs were not a factor, but the right kidney and the spinal cord lay distal to the target volume. As in the superior slices, the target volume was relatively shallow. The lack of a sharp slope in the target volume's distal surface lead to a smoother shaped bolus, and the dose to the target volume was similar both with and without the bolus. The 50 Gy isodose contour very closely matched the target volume in the bolus plan. In the bolus plan, there was a reduced dose to the right kidney, which had a significant volume that received in excess of 25 Gy if no bolus was used, but a negligible volume in excess of 25 Gy in the presence of a bolus. Moreover, the spinal cord received a dose in excess of 50 Gy if no bolus was used, compared with a dose of less than 40 Gy with a bolus.

In addition to using isodose curves, the usefulness of a bolus was assessed by comparing DVHs of the target volume and critical structures for both bolus and no-bolus treatments. Figures 5a–5e compare cumulative DVHs of the plans with and without a bolus for the target volume, spinal cord, both lungs, and the right kidney.

Figure 5a shows the DVH for the target volume. For both plans, a small amount (less than 5%) of the target

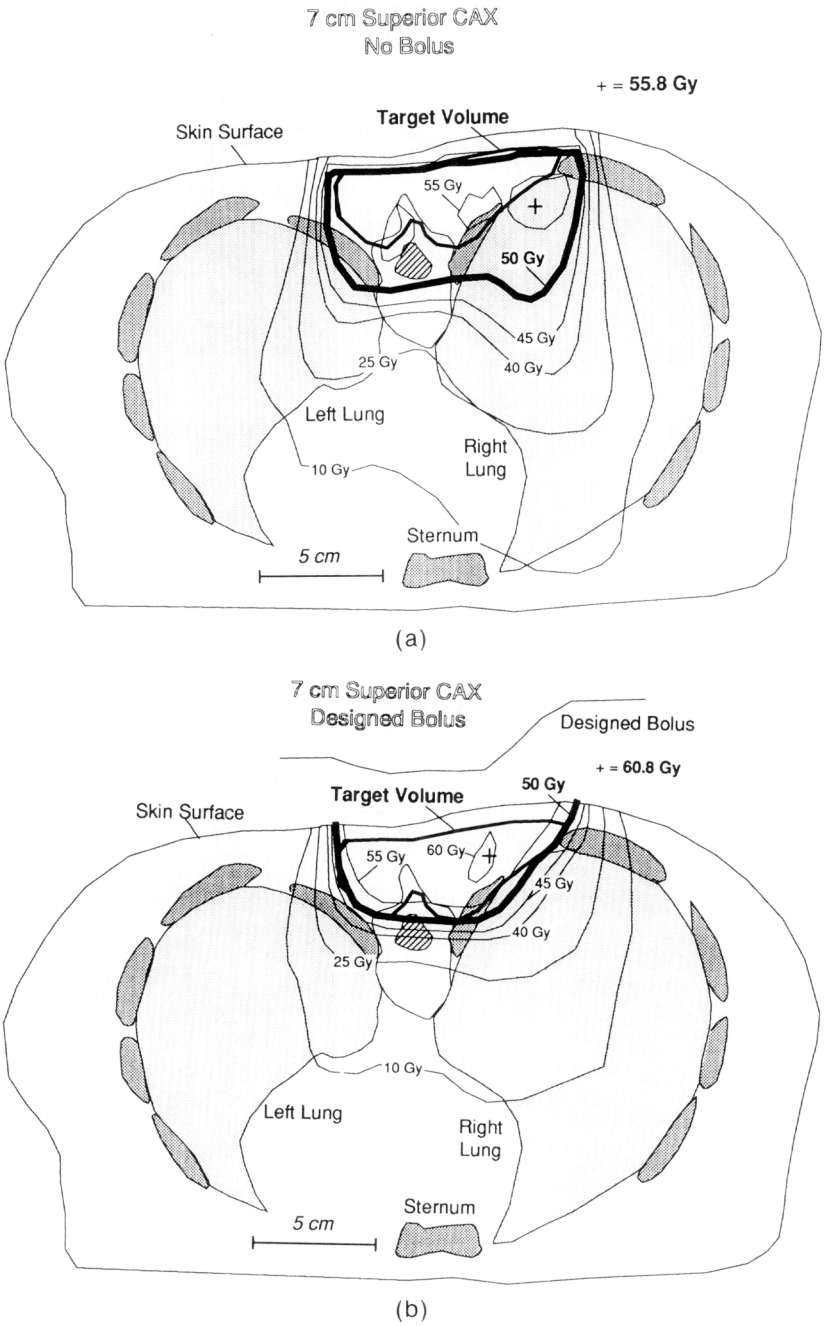

Fig. 3. Comparison of the dose distributions in the transverse plane lying 7 cm superior to the central axis. The position of the point of highest dose is identified with a +, and the dose at this point is indicated. (a) The dose distribution was calculated without a bolus. (b) The dose distribution was calculated with the designed bolus.

volume received a dose less than the desired 50 Gy. This underdosed region occurred at the perimeter of the target volume and was caused by an inadequate lateral margin between the target volume and the edge of the treatment portal. This was not considered clinically significant. For both plans, the dose to the target volume did not exceed the limit of 61 Gy; however, the dose gradient across the target volume was greater in the bolus plan. The increased dose spread in the bolus plan is a direct result of the irregular surface of the bolus modifying the electron scatter. The overlying bolus provides more buildup (due to electron scatter), which tends to increase dose in the underlying tumor volume. Also, because the bolus surface is sloped, dose inhomogeneities are generated due to changes in lateral scatter equilibrium, tending to increase the dose near the bolus surface and decreasing it distally (4). Because the bolus thickness varies, the dose variation across the target volume increases. Nonetheless, both plans were considered clinically equivalent in meeting the dose requirements for the target volume.

Figure 5b shows the DVH for the spinal cord. In the no-bolus plan, approximately 55% of the irradiated cord (defined as cord receiving more than 1 Gy) received a dose in excess of 45 Gy, whereas less than 5% of the

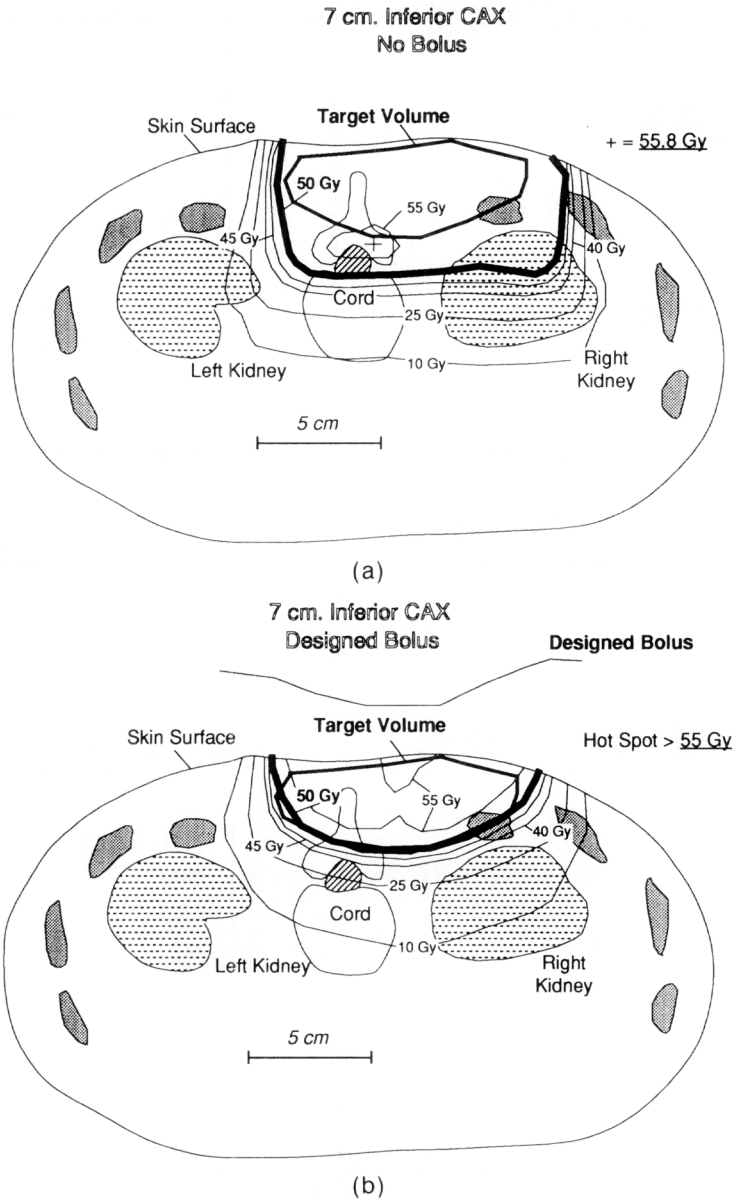

Fig. 4. Comparison of dose distributions in the transverse plane lying 7 cm inferior to the central axis. The position of the point of highest dose is identified with a +, and the dose at this point is indicated. (a) The dose distribution was calculated without a bolus. (b) The dose distribution was calculated with the designed bolus.

irradiated cord received this dose in the bolus plan. The no-bolus plan was clearly unacceptable because of the potential overirradiation of the spinal cord; this problem was cured by the application of a bolus.

Figures 5c and 5d show the DVHs for the left and right lungs, respectively. In both lungs, the bolus plan delivered significantly less dose than did the no-bolus plan. The total digitized right-lung volume was 1300 cm^3, and the amount of right lung receiving more than 20 Gy was approximately 450 cm^3 in the no-bolus plan and approximately 220 cm^3 in the bolus plan. Significantly less lung damage would be expected to result from the bolus plan.

Figure 5e shows the DVH for the right kidney. The total digitized right-kidney volume was 126 cm^3. The no-bolus plan irradiated 58 cm^3 of the right kidney to a dose in excess of 25 Gy, whereas a negligible fraction of kidney was irradiated in excess of 25 Gy in the bolus plan.

Verification of fabricated bolus

To verify the accuracy of the bolus fabrication process, the bolus shape and the resulting dose distribution for the designed and fabricated bolus are compared. Figures 6, 7, and 8 illustrate dose distributions of only the electron beam in transverse planes 7 cm superior to, directly on, and 7 cm inferior to the central axis, respectively. Isodose contours indicate the percentage of the dose relative to a reference dose defined as the dose delivered to central axis d_{max} for the rectangular field circumscribing the actual treatment field (given dose). Figures 6a through 8a show the designed bolus and resulting dose distributions, while

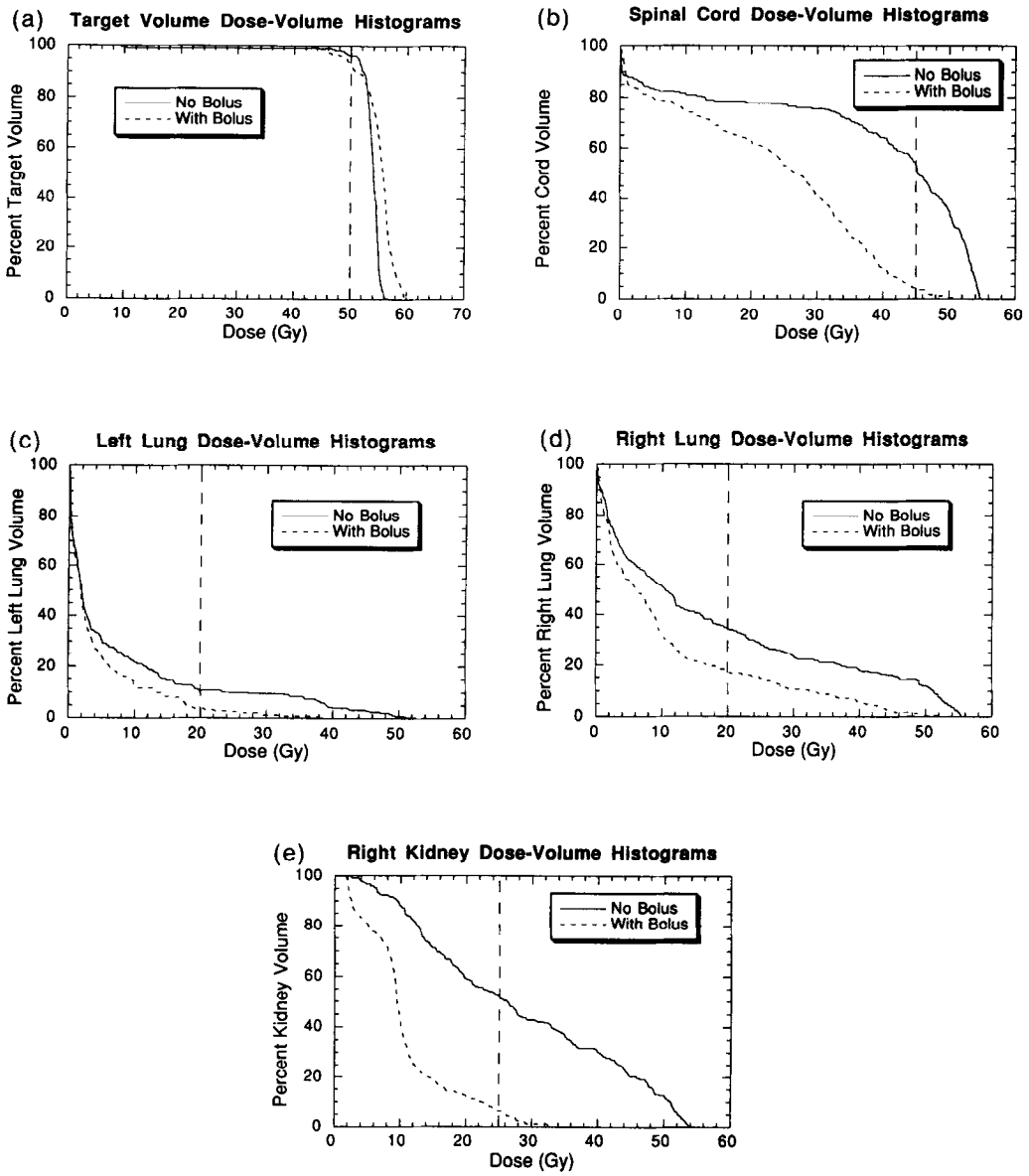

Fig. 5. Comparison of DVHs in the absence of bolus (solid line) with DVHs with the designed bolus (dashed line) for (a) target volume, (b) spinal cord, (c) left lung (total volume = 1010 cm^3), (d) right lung (total volume = 1300 cm^3), and (e) right kidney (total volume = 126 cm^3).

Figs. 6b through 8b show the fabricated bolus and resulting dose distributions. The quality of the bolus manufacturing process was tested by its ability to provide the same bolus thickness and dose distribution as that of the designed bolus. Comparing the bolus thicknesses of the transverse planes in Figs. 6 through 8 shows the accuracy in the bolus fabrication process. Over most of the bolus, the accuracy of bolus thickness resulting from the manufacturing process was better than 0.4 cm. The accuracy was limited, in part, by the spatial density of the calculated bolus-surface arrays transferred from the 3D-RTP system being limited by the milling software. The bolus arrays were interpolated; hence, the surfaces they define did not precisely agree with those designed by the 3D-RTP system.

Some differences were noted between the dose distributions of the designed bolus and those obtained from the CT scan with the fabricated bolus. These were believed to be due, in part, to differences in patient orientation and to a slight growth of the tumor in the time between the two sets of CT images. The differences were not large, however, as can be observed by the relationship between certain isodoses and physical features such as the spinal cord. The position shifts of the isodoses at depth were typically less than 0.4 cm. A more automated method for bolus verification is presently under investigation.

The conformation of the prescription isodose with the target volume and the constraint of dose to critical structures is a function of the accuracy of the dose calculation algorithm and the reproducibility of the patient setup. For this

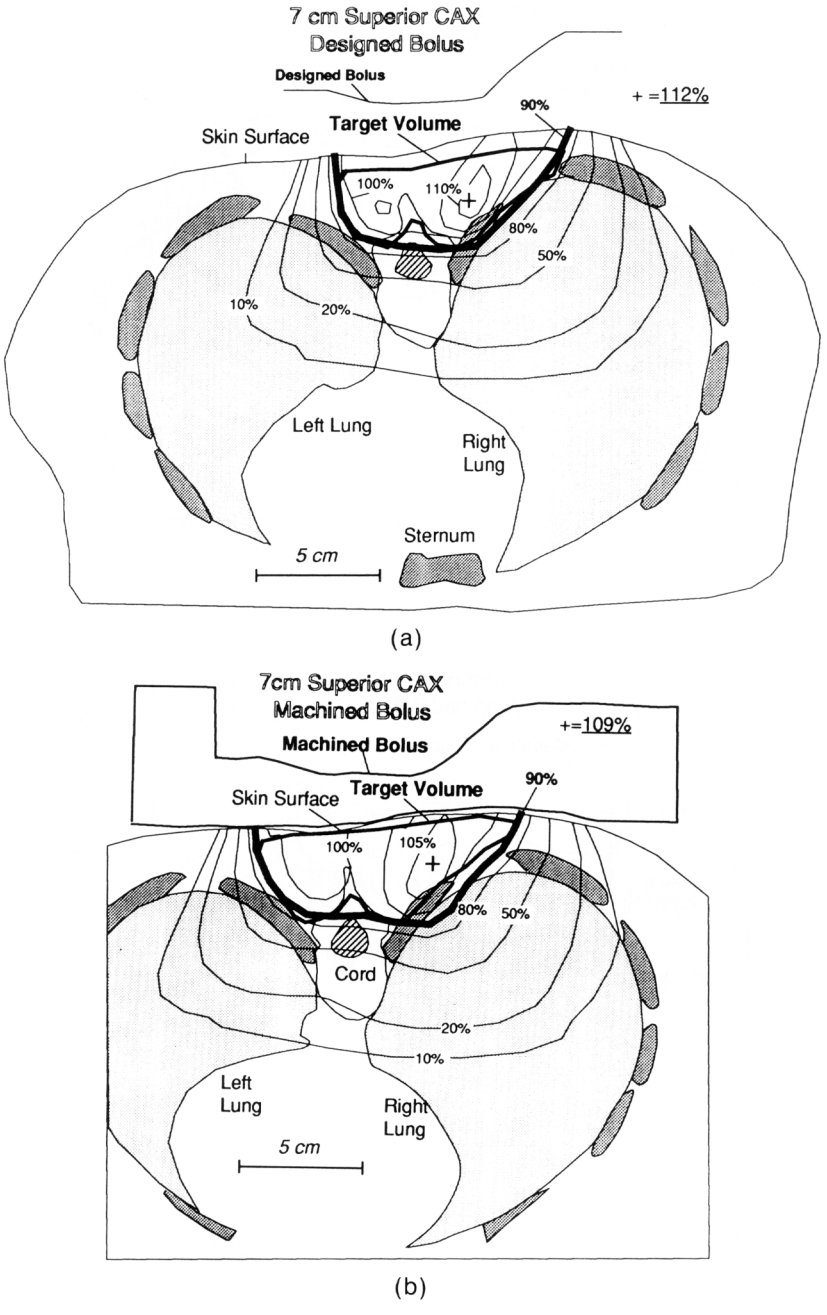

Fig. 6. Anatomical structures and the electron-beam isodose distribution for the transverse plane lying 7 cm superior to the central axis of the beam. The position of the point of highest dose is identified with a +, and the dose at this point is indicated. (a) The CT image used for this calculation was taken prior to the manufacturing of the bolus. The dose distribution was calculated with the designed bolus. (b) The CT image used for this calculation was taken with the fabricated bolus in place.

patient treatment, the two major concerns are the dose to the target volume and to the spinal cord. Uncertainties in dose to the target volume are primarily due to inaccuracies in the dose algorithm, error in bolus fabrication, and error in bolus alignment. Regarding the dose algorithm, Shiu *et al.* (12) have studied the dose accuracy for a variety of geometries simulating patient treatments at two beam energies using a standard data set (13). The most comparable data set, a 20 MeV beam incident on a 30° angulated surface, shows the dose calculated in the target volume to be accurate to within 5%. Inaccuracies in dose resulting from errors in bolus fabrication have been the subject of separate research by Bawiec (2) for which one study was bolus in treating the paraspinal muscles. That study compared dose for the designed with dose for the fabricated bolus, showing accuracies of ±2% for 70% of the dose points and ±5% for greater than 99% of the dose points. No data exists specifically studying bolus misalignment; however, the results of the present work reflect a combination of bolus fabrication and alignment error.

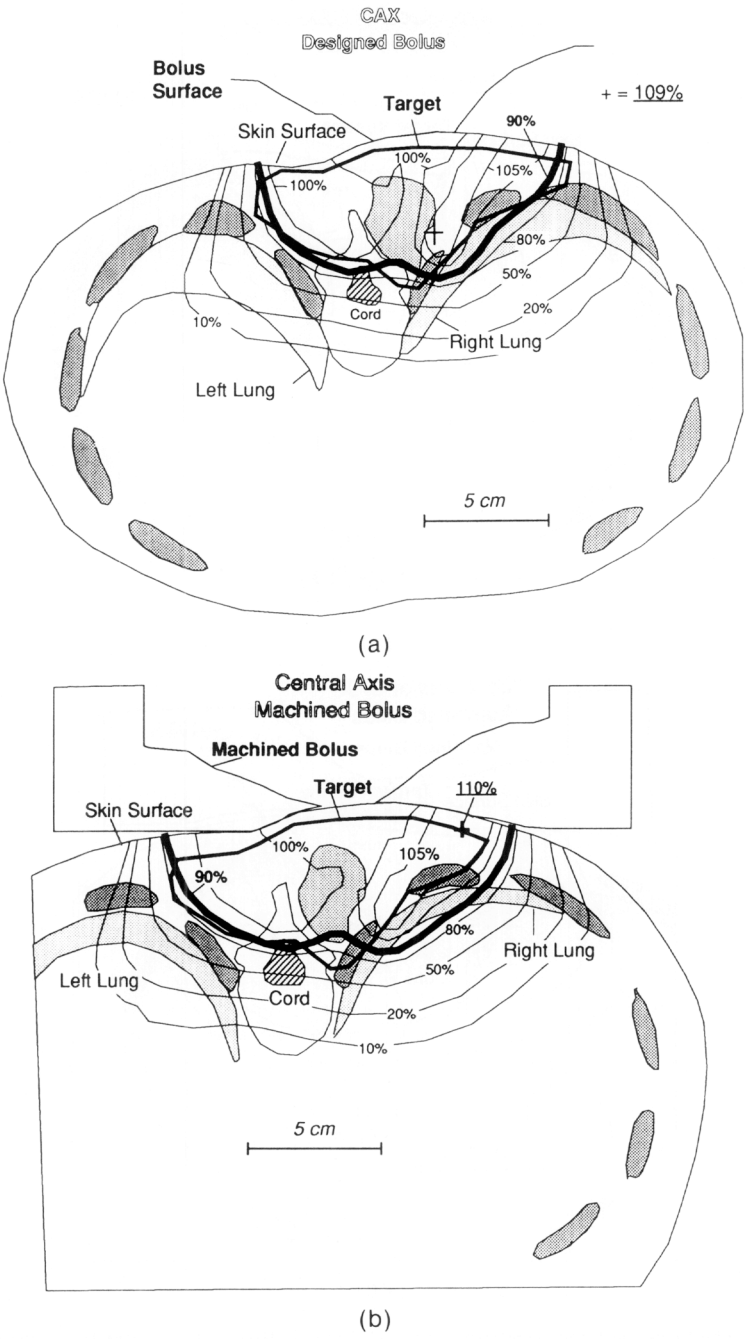

Fig. 7. Anatomical structures and the electron-beam isodose distribution for the transverse plane containing the central axis of the beam. The position of the point of highest dose is identified with a +, and the dose at this point is indicated. (a) The CT image used for this calculation was taken prior to the manufacturing of the bolus. The dose distribution was calculated with the designed bolus. (b) The CT image used for this calculation was taken with the fabricated bolus in place.

The major concern regarding dose inaccuracy due to internal inhomogeneities would be dose to the spinal cord. Dominiak (3) studied inaccuracy of calculated dose to the spinal cord when it was being treated with 15 MeV electrons for treatment of base of brain tumors. Results showed the measured cord dose to be as much as 0 to 8% greater than that calculated by the pencil-beam algorithm. While these uncertainties will affect the individual DVHs, the difference between the DVH with and without bolus will still be significant.

Follow-up

At surgery an $8 \times 5 \times 3$ cm^3 tumor was resected with negative margins. One and one-half years later the patient presented with a bony metastasis to the right-orbital region. This was treated with chemotherapy (four cycles of ifosfamide with GCSF support). Three and one-half years after her initial radiotherapy, the patient returned with a 3-month history of groin and lower back pain. Initial radiographic examination was negative, but 2 months later the patient had a positive bone scan at the femur

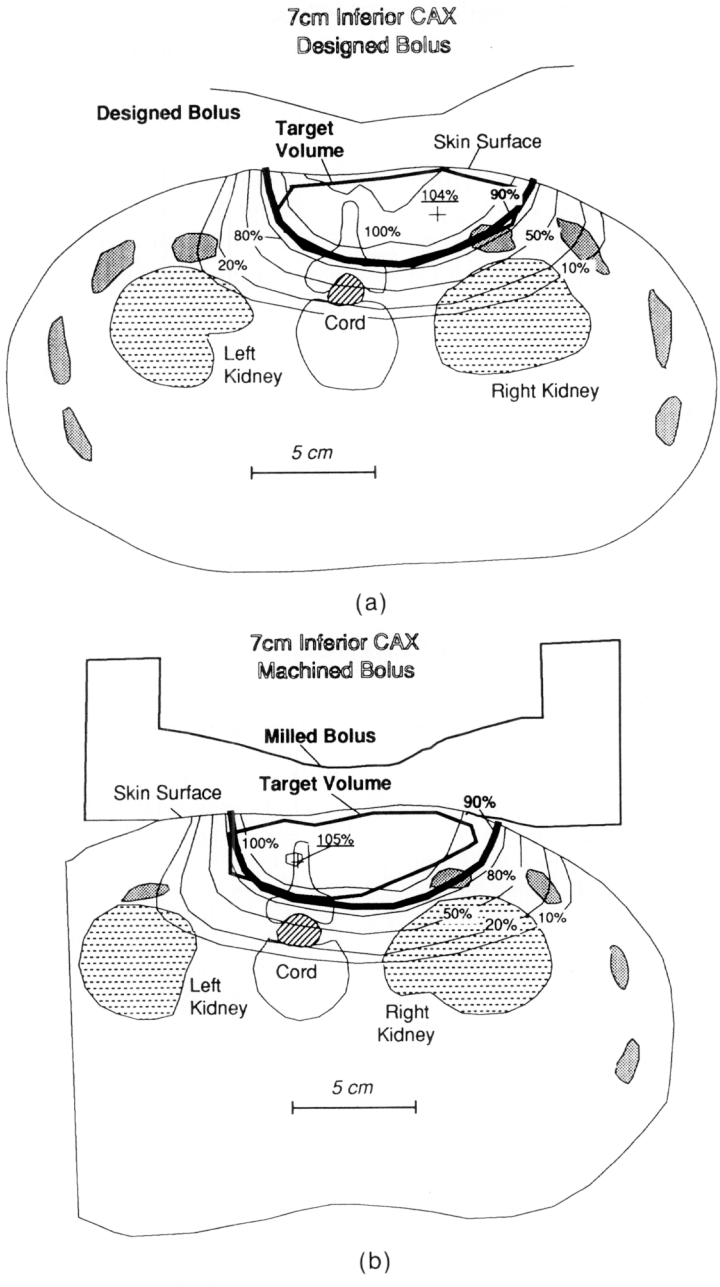

Fig. 8. Anatomical structures and the electron-beam isodose distribution for the transverse plane lying 7 cm inferior to the central axis of the beam. The position of the point of highest dose is identified with a +, and the dose at this point is indicated. (a) The CT image used for this calculation was taken prior to the manufacturing of the bolus. The dose distribution was calculated with the designed bolus. (b) The CT image used for this calculation was taken with the fabricated bolus in place.

acetabulum and a positive MRI of the pelvis. The patient was treated with VP16. Four years after completion of the original radiotherapy, the patient was alive with metastatic disease, and physical examination revealed a 2–3 cm diameter tumor in the right lower back that recurred within the radiation field. Due to the patient's poor clinical status, no additional diagnostic examinations were performed.

CONCLUSIONS

This work demonstrated the usefulness and quality of a new bolus design and fabrication system through the application of this system to the treatment of a chondrosarcoma. The design algorithms yielded a bolus that provided similar target-volume coverage, while supplying significantly improved sparing of distal critical structures relative to the plan that did not use an electron bolus. The no-bolus electron plan, which was clinically unacceptable, was made acceptable through the use of bolus. Both the bolus and no-bolus plans delivered the prescribed dose to 95% of the target volume. The bolus plan had a slightly greater spreading in the dose distribution, with the average dose to the target volume increasing slightly, by 1.6 Gy (2.9%), when the bolus was added. There were sig-

nificant reductions in dose to the critical structures with the use of a bolus. The fraction of irradiated cord that received a dose greater than 45 Gy decreased from approximately 55 to 5% with the use of a bolus. The volume of right lung that received a dose in excess of 20 Gy was approximately 230 cm^3 less in the bolus plan. Fifty percent of the kidney received a dose in excess of 25 Gy in the no-bolus plan compared with less than 7% in the bolus plan. The bolus was useful because it allowed for a marked reduction in the doses to the critical structures without significantly compromising the dose to the target volume.

On the other hand, the patient had a history of metastatic disease and ultimately presented with a recurrent tumor in the treatment field approximately four years later. These results emphasize the need to understand the spread of microscopic disease relative to its anatomic location, especially when localized disease is being treated with conformal radiotherapy. Such concerns will be important for future clinical studies of electron bolus used in treatment of sarcomas of the paraspinal muscles.

A method for verification of the bolus design and fabrication methods was demonstrated. The patient underwent CT scanning with the fabricated bolus in place, and the resulting dose distribution in the patient was calculated. The CT scan showed that the bolus fabrication system, which used a computer-driven milling machine, machined the bolus with an overall accuracy of bolus thickness and distal surface shape of less than approximately 0.4 cm. Dose distributions with the designed bolus and fabricated bolus were compared, and isodose contours were found to agree to within a few millimeters, providing additional confidence in the bolus fabrication process. This method shows promise as a quality-assurance tool; development to further automate the process of bolus shape and dose comparison is in progress (2).

REFERENCES

1. Antolak, J. A.; Starkschall, G.; Baiwec, E. R.; Ewton, J. R.; Hogstrom, K. R. Implementation of an automated electron bolus fabrication system for conformal electron radiotherapy. In: Proceedings of the XIth International Conference on The Use of Computers in Radiation Therapy. Manchester, UK: Handley Printers Ltd.; 1994:162–163.
2. Bawiec, E. R. The effects of accuracy in milling of electron bolus on dose delivery. M. A. Thesis, U.T. Health Science Center at Houston, Graduate School of Biomedical Sciences; 1994.
3. Dominiak, G. S. Dose in spinal cord following electron irradiation. M. A. Thesis, U.T. Health Science Center at Houston, Graduate School of Biomedical Sciences; 1991.
4. Estrand, K. E.; Dixon, R. L. The problem of obliquely incident beams in electron-beam treatment planning. Med. Phys. 9:276–278; 1982.
5. Hogstrom, K. R.; Fields, R. S. Use of CT in electron beam treatment planning: Current and future development. In: Ling, C. C., Rogers, C. C., Morton, R. J., eds. Computed Tomography in Radiation Therapy. New York: Raven Press; 1983:223–243.
6. Hogstrom, K. R.; Mills, M. D.; Almond, P. R. Electron beam dose calculations. Phys. Med. Biol. 26:445–459; 1991.
7. Hogstrom, K. R.; Smith, A. R.; Simon, S. L.; Somers, J. W.; Lane, R. G.; Rosen, I. I.; Kelsey, C. A.; von Essen, C. F.; Klingerman, M. M.; Berardo, P. A.; Zink, S. M. Static pion beam treatment planning of deep seated tumors using computerized tomographic scans at LAMPF. Int. J. Radiat. Oncol. Biol. Phys. 5:875–886; 1979.
8. Low, D. A.; Hogstrom, K. R. Determination of the relative linear collision stopping power and linear scattering power of electron bolus material. Phys. Med. Biol. 39:1063–1068; 1994.
9. Low, D. A.; Starkschall, G.; Bujnowski, S. W.; Ewton, J. R.; Hogstrom, K. R. Computer-aided design, fabrication and verification of bolus for electron-beam radiotherapy. (Abstr.) Med. Phys. 17:732; 1990.
10. Low, D. A.; Starkschall, G.; Bujnowski, S. W.; Wang, L. L.; Hogstrom, K. R. Electron bolus design for radiotherapy treatment planning: Bolus design algorithms. Med. Phys. 19:115–124; 1992.
11. Niemierko, A.; Goitein, M. Random sampling for evaluating treatment plans. Med. Phys. 17:752–762; 1990.
12. Shiu, A. S.; Starkschall, G.; Buknowski, S. W.; Hogstrom, K. R. Evaluation of a 3D electron pencil beam algorithm by comparison with measured data. (Abstr.) Med. Phys. 16:490; 1989.
13. Shiu, A. S.; Tung, S.; Hogstrom, K. R.; Wong, J. W.; Gerber, R. L.; Harms, W. B.; Purdy, J. A.; Ten Haken, R. K.; McShan, D. L.; Fraass, B. A. Verification data for electron beam dose algorithms. Med. Phys. 19:623–636; 1992.
14. Smith, R. M.; Galvin, J. M.; Needham, M.; Smith, A. Computer-aided design and fabrication of electron compensation bolus. (Abstr.) Med. Phys. 16:455; 1989.
15. Starkschall, G.; Bujnowski, S. W.; Wang, L. L.; Low, D. A.; Hogstrom, K. R. Effect of dimensionality of heterogeneity corrections on the implementation of a three-dimensional electron pencil-beam algorithm. Phys. Med. Biol. 36:207–227; 1991.
16. Starkschall, G.; Bujnowski, S. W.; Wang, L. L.; Shiu, A. S.; Boyer, A. L.; Desobry, G. E.; Wells, N. H.; Baker, W. L.; Hogstrom, K. R. A full three-dimensional radiotherapy treatment planning system. (Abstr.) Med. Phys. 18:647; 1991.
17. Wagner, M. S. Automated range compensation for proton therapy. Med. Phys. 9:749–752; 1982.
18. Zhu, Y.; Boyer, A. L. X-ray dose computations in heterogeneous media using 3-dimensional FFT convolution. Phys. Med. Biol. 35:351–368; 1990.